Journal of Materials Chemistry

Cite this: *J. Mater. Chem.*, 2011, **21**, 5972

www.rsc.org/materials

PAPER

Graphene sheets decorated with SnO_2 nanoparticles: *in situ* synthesis and highly efficient materials for cataluminescence gas sensors†

Hongjie Song, Lichun Zhang, Chunlan He, Ying Qu, Yunfei Tian and Yi Lv*

Received 11th December 2010, Accepted 16th February 2011
DOI: 10.1039/c0jm04331a

Graphene sheets decorated with SnO_2 nanoparticles were prepared through a facile hydrothermal-assisted *in situ* synthesis route. According to the XPS, XRD, FESEM and TEM analysis, rutile SnO_2 nanocrystals were exclusively deposited on graphene sheets with high density and high uniformity to form layered composite sheets. Propanal, a common volatile organic compound, was selected as a model to investigate the cataluminescence (CTL) sensing properties of the SnO_2/graphene composite in this paper. It was found that the strong CTL emission could be generated due to the catalyzing oxidization of propanal on the surface of SnO_2/graphene composite and this composite was an efficient sensing material for propanal. We further studied the analytical characteristics of the CTL sensor based on SnO_2/graphene composite sensing material for propanal under the optimal experimental conditions. The linear range of the propanal gas sensor was 1.34–266.67 μg mL^{-1} ($r = 0.9987$), over two orders of magnitude, and the detection limit was 0.3 μg mL^{-1}($S/N = 3$).

1. Introduction

Graphene, a two-dimensional monolayer of fused sp^2 carbon bonds in a honeycomb-like network, has attracted a great deal of scientific interest not only in basic scientific studies[1–4] but also potential applications,[5–7] which is mainly attributed to its outstanding mechanical, electrical, thermal, and optical properties and theoretically high surface area of ~2600 m^2 g^{-1}.[8] The unique, outstanding physicochemical properties depends strongly on the number of layers and the dispersion performance of graphene sheet.[9] However, Van der Waals and π–π stacking interactions among individual graphene sheets result in their tendency to aggregate[10,11] when graphene dispersion solutions are dried. By incorporation of nanoparticles into graphene sheets, in addition to the good distribution of nanoparticles, the aggregation problem of graphene sheets could be minimized or prevented.[9] Therefore, graphene sheets decorated with nanoparticles combine the outstanding properties of them and might result in some particular properties because of the synergetic effect between them. With this in mind, graphene decorated with metal nanoparticles[11–20] and metal oxides nanoparticles[10,21–29] have recently been reported. Among the metal oxide nanoparticles decorating graphene, intensive attention should be paid to SnO_2 nanoparticles because of their unique properties such as high optical transparency, electrical conductivity and chemical sensitivity. To date, there have been a few reports about the preparation of SnO_2/graphene composites with application in lithium batteries[25,30–32] or supercapacitors,[21] it is still essential to develop new methods and applications of SnO_2/graphene composites.

The demand for low-cost, low-power, and portable volatile organic compounds (VOCs) detection is increasing dramatically due to the increasing attention to environmental monitoring, space exploration, homeland security, agriculture, and medical applications.[33] Sensors based on cataluminescence (CTL) refers to the kind of chemiluminescence (CL) that is emitted during the catalysis of organic vapors on the surface of solid catalysts in an atmosphere containing oxygen and have been proved effective to meet this demand.[34–39] As to the development of CTL-based sensors, one of the most difficult challenges is to find specific materials that have both high sensitivity and good selectivity for the substances to be detected. The graphene sheets decorated with metal oxide nanoparticles, which with good distribution can provide greater versatility in carrying out adsorption, selective catalytic and sensing processes, has more porosity and large specific surface area which are attractive advantages for CTL sensing materials. Therefore graphene/metal oxide composites may provide new opportunities to develop new CTL sensing materials.

Herein, we report a hydrothermal-assisted *in situ* route to synthesize graphene sheets decorated with SnO_2 nanoparticles, meanwhile, the application of this composite in cataluminescence sensor was investigated. The greatest advantage of this method is that graphene sheets and SnO_2 nanoparticles are formed at the

Key Laboratory of Green Chemistry & Technology, Ministry of Education, College of Chemistry, Sichuan University, Chengdu, Sichuan, 610064, China; Web: . E-mail: lvy@scu.edu.cn; Fax: +86 28 85412798; Tel: +86 28 85412798

† Electronic supplementary information (ESI) available: Details of the preparation of graphite oxide, O1s XPS analysis, TEM image and corresponding SAED pattern of pure SnO_2, CTL response profiles and optimal CTL sensing conditions. See DOI: 10.1039/c0jm04331a

same time *via* the hydrothermal-assisted *in situ* oxidation-reduction reaction between graphene oxide and $SnCl_2$ in the presence of HCl and urea. We further designed a new CTL sensor for propanal based on the phenomenon that strong CTL emission could be generated due to the catalyzing oxidization of propanal on the surface of SnO_2/graphene composite. CTL sensing measurements prove that this composite has both high sensitivity and good selectivity to propanal.

2. Experimental section

2.1 Chemical reagents and materials

Graphite powder was specpure grade and obtained from Tianjin Guangfu Fine Chemical Research Institute. The other chemicals were all analytical grade and used without further purification. P_2O_5, H_2SO_4, $K_2S_2O_8$, $KMnO_4$, H_2O_2 (30%), HCl, $SnCl_2 \cdot 2H_2O$, urea, propanal, ethanol, and acetone were obtained from Chengdu Kelong Chemical Reagent Company (China). HRTEM micrographs were obtained on a 200 mesh holey carbon supported copper grids.

2.2 Preparation of graphene sheets decorated with SnO_2

Graphite oxide was synthesized from graphite powder by a modified Hummers' method[7] (the preparation of graphite oxide, ESI†). Graphite oxide (10 mg) was exfoliated in distilled water (20 mL) with ultrasonic treatment to form a colloidal suspension. $SnCl_2 \cdot 2H_2O$ (1.30 g) was dissolved in HCl (38%, 0.7 mL) with distilled water (20 mL) added forming a $SnCl_2$–HCl solution. The above colloidal suspension and $SnCl_2$–HCl solution were mixed with urea (1.30 g) under vigorous stirring to form a uniform solution. After 30 min of ultrasonic treatment, the resultant solution was then transferred into a Teflon-lined stainless steel autoclave (50 mL) and maintained at 353 K for 12 h. The solid products were collected by filtered through 0.22 μm filter and washed with distilled water. The precipitate was dried at 353 K overnight.

2.3 Characterization and apparatus

The surface composition and chemical states of product was analysed by X-ray photoelectron spectroscopy (XPS), the morphology, dimension and structure were characterized by X-ray diffraction (XRD), field emission scanning electron microscopy (FESEM), transmission electron microscopy (TEM) and high resolution transmission electron microscopy (HRTEM). For the XPS analysis, a XSAM 800 Electron Spectrometer (Kratos) was used with using monochromatic Al K_α radiation (1486.6 eV). The powder X-ray diffraction patterns were recorded with a X' Pert Pro X-ray diffractometer (Philips) with Cu-Kα radiation ($\lambda = 1.5406$ Å), using an operation voltage of 40 kV and a current of 35 mA, respectively. FESEM image was obtained on a Hitachi S3400 field emission scanning electron microscope operated at 20 kV. The TEM, magnified HRTEM images and corresponding SAED were obtained from a Tecnai G^2 F20 S-TWIN (FEI) HRTEM measurements at an accelerating voltage of 200 kV.

2.4 Cataluminescence sensing measurements

The cataluminescence sensing characteristic of the as-prepared graphene sheets decorated with SnO_2 in response to propanal was tested by a CTL system as described in previous work.[37] The CTL sensor reaction cell linked up with a voltage controller was homemade. Briefly, about 0.03 g SnO_2/graphene composite used as sensing material were coated as a layer on a ceramic heating tube which was put into a quartz tube (i.d. = 6 mm and length = 95 mm). The CTL spectra was measured by a flow-injection chemiluminescence analyzer (IFFD, Xi'an Remax Electronic Science Tech. Co. Ltd., Xi'an, China), which was operated by a computer. The photomultiplier tube (PMT) used in this analyzer was operated in current mode and potential supply of the photomultiplier tube was 600 V. The sample gas was delivered by the steady air carrier stream from an air pump and then reached the reaction cell, the consequent CTL emission was monitored by IFFD analyzer.

3. Results and discussion

3.1 Preparation and characterization of graphene sheets decorated with SnO_2 nanoparticles

In this work, we adopted a convenient *in situ* method to fabricate graphene sheets decorated with SnO_2 nanoparticles based on the oxidation–reduction reaction between graphene oxide and $SnCl_2 \cdot 2H_2O$. In order to suppress the hydrolysis of $SnCl_2$, we dissolved $SnCl_2 \cdot 2H_2O$ (1.30 g) in HCl (38%, 0.7 mL) followed by adding distilled water (20 mL). The $SnCl_2$–HCl solution was transparent, indicating that tin composition exists as Sn^{2+} cations in the solution. In the chemical synthesis process, firstly, graphene oxide sheets with large quantity of carboxylic acid groups on the edge sites and epoxyl, hydroxyl moieties on the basal plane[40] were dispersed in water, forming a uniform dispersion solution because of these oxygenate species. When graphene oxide sheet solution was mixed with $SnCl_2$–HCl solution, the Sn^{2+} cations were attracted and anchored on those functional groups through electrostatic attraction.[26,41] Graphene oxide sheets can be considered as macromolecules, therefore, the mixing of Sn^{2+} and graphene oxide sheets can be considered as at molecular level.[42] Due to the reducing property of $SnCl_2$ in acid solution, graphene oxide sheets were converted to graphene sheets and the anchored Sn^{2+} ions were converted to SnO_2 respectively, large quantity of oxygenate species and dispered graphene sheets could lead to the continuously oxidation of the Sn^{2+} in solution. The possible formation reaction mechanism of SnO_2 phase and graphene can be ascribed by the following reactions:

$$SnCl_2 + \text{graphene oxide} + H_2O \rightarrow SnO_2 + \text{graphene} + 2HCl \quad (1)$$

$$CO(NH)_2 + 3H_2O \rightarrow CO_2\uparrow + 2NH_4OH \quad (2)$$

$$NH_4OH + HCl \rightarrow NH_4Cl + H_2O \quad (3)$$

Hydroxide ion liberated uniformity during the decomposition of urea under hydrothermal conditions could neutralize HCl produced by reaction (1), which helped to complete the oxidation–reduction reaction between Sn^{2+} and graphene oxide. This

process could ensure the *in situ* formation of SnO_2 nanoparticles with uniformity and graphene sheets simultaneously, with an advantage to decrease the serious stacking of graphene sheets and prevent the agglomeration of SnO_2 nanoparticles.

Fig. 1 shows the typical X-ray diffraction (XRD) pattern of the as-prepared SnO_2/graphene composite, clearly suggestive of a tetragonal rutile structure (JCPDS card no. 41-1445). The highly broadened diffraction peaks are indicative of the formation of SnO_2 nanocrystals with very small size. These results are also confirmed by HRTEM as described later. No obvious peaks corresponding to graphene are observed in the powder pattern, which might attribute to the following reasons: (1) the disordered interfacial structure produced by the interfacial bonds between SnO_2 nanocrystals and graphene sheets; (2) the low amount of graphene sheets in the SnO_2/graphene composite (the chemical analysis reveals that the weight percent of the SnO_2 nanoparticles is about 80%); (3) the disordered stacking nature of graphene sheets in the composite.

XPS analysis was conducted in the region of 0–1100 eV to investigate the surface composition and chemical states of the species in the SnO_2/graphene composite. Fig. 2a shows the wide-survey XPS spectra of the composite, which reveals the presence of carbon, oxygen and tin, no other hetero elements were detected. The Sn 3d spectrum, as shown in Fig. 2b, two symmetrical peaks at 487.0 eV and 495.5 eV are attributable to Sn $3d_{5/2}$ and Sn $3d_{3/2}$, respectively, which is in good agreement with the energy splitting reported for SnO_2.[42,43] The peak-to-peak separation between the Sn $3d_{5/2}$ and Sn $3d_{3/2}$ level is 8.5 eV, and the area ratio of the two peaks is 1.5, which are approximately the same values as those reported in the XPS spectrum of SnO_2. The presence of SnO_2 can be further confirmed by the O 1s XPS peak at 530.8 eV (Fig. S1, ESI†), which corresponds to the oxygen species in the SnO_2. Fig. 2c and 2d display the high-resolution spectra of the C 1s region of graphene oxide and SnO_2/graphene composite, respectively. The C 1s spectrum of GO contains four components: the nonoxygenated ring C (284.7 eV), C–OH species (286.7 eV), C═O species (287.9 eV) and C═O–OH (289.1 eV). The C 1s spectrum of SnO_2/graphene composite reveals that, compared to graphene oxide, relative contribution

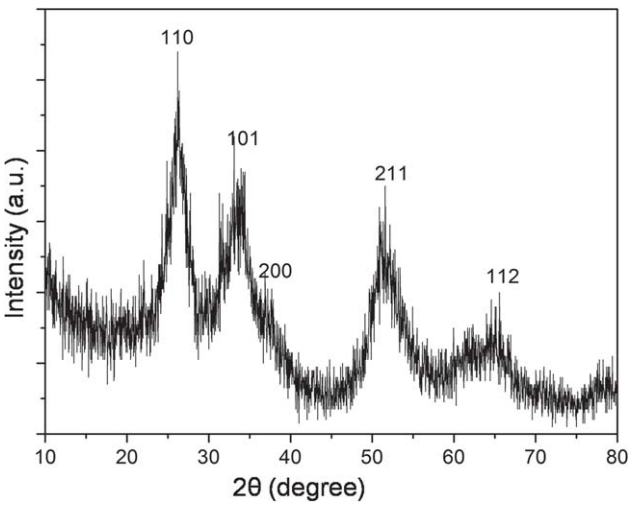

Fig. 1 XRD pattern of the prepared SnO_2/graphene composite.

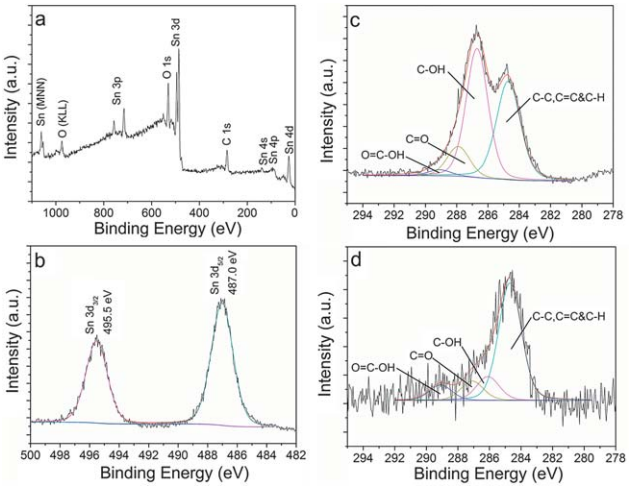

Fig. 2 XPS spectrum (a) and Sn 3d XPS spectrum (b) of SnO_2/graphene composite. C 1s XPS spectra of graphene oxide (c) and SnO_2/graphene (d), respectively.

of the components associated with oxygenated functional groups decreased markedly, indicating the reduction of graphene oxide to graphene in the hydrothermal reaction. Due to the low reducibility of $SnCl_2$, there still has small amount residual oxygenated groups left which is also confirmed by the O 1s XPS peaks at 531.7 eV and 532.3 eV in Fig. S1 (ESI†), however, the remaining small amount oxygenated groups help to maintain the high dispersion of SnO_2 nanocrystals on graphene sheets through hydrogen bonding and electrostatic attraction.

The morphology and structural features of SnO_2/graphene composite were elucidated by FESEM, TEM and HRTEM

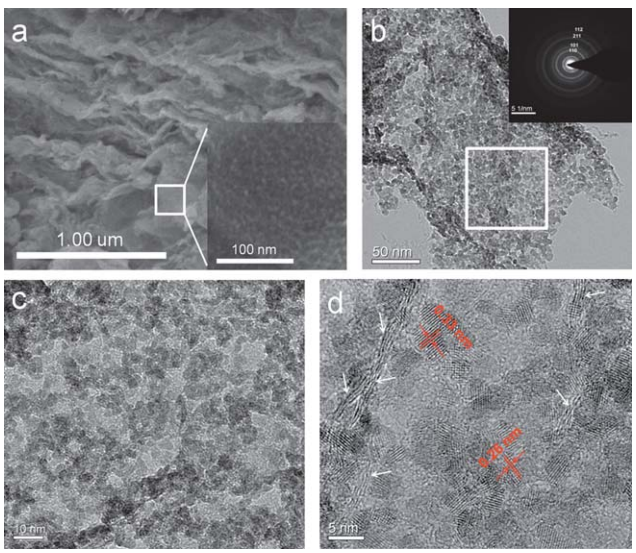

Fig. 3 (a) FESEM image of SnO_2/graphene composite from the edge-side view, the inset is the high magnification of the approximate area outlined with the white rectangle. (b) Low-magnification TEM and the corresponding selected-area electron diffraction (SAED) pattern shown in the inset. (c) High-magnification TEM of the approximate area outlined with the white rectangle in (b). (d) The cross-sectional high-magnification TEM image of SnO_2/graphene composite.

analyses. Fig. 3a presents the representative FESEM image of the composite from the edge-side view, showing the layered platelets composed of curled nanosheets. Small SnO_2 nanoparticles are homogeneously distributed on graphene sheets, as elucidates in the high magnification (the inset in Fig. 3a) of the approximate area part outlined in white rectangle. Due to the reassembling process between graphene sheets and SnO_2 nanoparticles, substantial voids exist between individual composite sheets, moreover, the decorated SnO_2 nanoparticles could act as a spacer to decrease the restacking and increases the stability of individual graphene sheets. The low-magnification TEM micrograph, as shown in Fig. 3b, indicates that SnO_2 nanoparticles are exclusively deposited on the flake-like graphene sheets with high density and high uniformity. These SnO_2 nanoparticles are firmly attached to graphene sheets, even after the ultrasonication used to disperse the SnO_2-graphene composite for TEM characterization. The corresponding selected-area electron diffraction (SAED) pattern (upper inset of Fig. 3b) shows typical diffraction rings indexed to tetragonal rutile SnO_2 nanocrystals phase. The detailed image of the approximate area outlined with the white rectangle in Fig. 3b is exhibited in Fig. 3c, which further reveals a good dispersion of SnO_2 nanocrystals with narrow size distribution on graphene sheets and the average particle size is 3–5 nm. Fig. 3d shows cross-sectional high-resolution TEM images of interfacial structure between SnO_2 nanocrystals and graphene sheets. It exhibits three distinct images: lines (marked by the arrowhead), "voids" and spherical shapes, the former is due to the stacked and curled graphene sheets of about 2–4 layers whereas the latter is from the SnO_2 nanocrystals surrounded by graphene sheets, the "voids" between them come from monolayer sheet that are not completely anchored by SnO_2 nanoparticles. The incomplete decoration results in substantial real voids between individual composite sheets during the reassembling process between graphene sheets and SnO_2 nanoparticles, which increases the sensing surface area and then improves the catalytic activity of this sensing material for pronanal oxidation. The disordered structure observed at the close interfacial region of SnO_2 nanoparticles and graphene sheets may suggest the formation of interfacial bonds which are propitious to the stabilization of SnO_2 nanoparticles decorating on graphene sheets. The aligned lattice fringes of the SnO_2 nanocrystals are also clearly illustrated in Fig. 3d, with adjacent fringe spacing of about 0.33 nm and 0.26 nm corresponding to the (110) plane and (101) plane of the rutile phase, respectively.

3.2 Cataluminescence application

Propanal, one of the most important volatile aldehydes, has been widely used in the chemical, medicine, paint, plastic, rubber, food and feed industries. It is not only harmful to human health, which may result in bronchitis, pneumonia and pulmonary edema, but also an important hazardous air pollutant with pungent smell and flammability. Highly sensitive and excellent selective methods for the determination of propanal are required. SnO_2 is an important material used for detecting flammable and toxic contaminants in many environments. Sensing characteristics of SnO_2 nanostructures for some gases have been investigated based on resistance change and CTL. Comparing to these resistance-based sensors with some problems such as poor selectivity, nonlinear response, and long-term drift, CTL-based sensors show some significant advantages, such as high sensitivity, good selectivity and fast response. With this in mind, SnO_2/graphene as CTL sensing material for propanal was investigated in this work.

The CTL sensing performance of the as-prepared SnO_2/graphene composite was evaluated by the responses of the CTL system to propanal with two different concentrations of 26.67 μg mL^{-1} and 133.33 μg mL^{-1}. A flow injection mode was applied to the present study by repeatedly injecting different volume propanal vapor into the carrier gas with the flow rate of 300 mL min^{-1} at 493 K. As shown in Fig. 4a, it is obvious that the SnO_2/graphene composite exhibits strong and steady CTL responses to propanal, the CTL intensity increases with the concentration of propanal. Moreover, both fast response time (within 5 s) and recovery time (within 30s) are seen from the typical CTL response profiles to propanal with three different concentrations in Fig. S2 (ESI†). Meanwhile, it can be found that the as-prepared composite as CTL sensing material shows an excellent selectivity towards propanal by investigating twenty sorts of common possible interfering substances, including formaldehyde, acetaldehyde, acetone, isopropanol, benzene, methanol, ethanol, carbon tetrachloride, ammonia, ethyl acetate, trichloromethane, acetonitrile, *tert*-butylamine, cyclohexane, dimethylbenzene, dichloromethane, n-pentane, n-hexane and water vapor under the same CTL test conditions with their concentrations of about 200 μg mL^{-1} at 573 K and the carrier gas with the flow rate of 300 mL min^{-1}, as displayed in Fig. 4b, there is no significantly interfere with detecting propanal. The high selectivity of composite towards propanal is possibly due to the following two aspects: (1) the specificity of sensing materials in cataluminescence reaction, meaning that a gas can be detected only when it can be catalytically oxidized on the catalyst and at the same time produces CL intermediates; (2) the structure and surface properties of the composite. As mentioned above, substantial voids exist between individual composite sheets, these voids can act as channel entrances for effectively controlled entry of reactant molecules that small molecular gases effuse from the voids quickly and gas molecules with large stereostructures have difficulty to enter the voids, resulting in less reaction opportunity with the adsorbed O_2 on the surface of individual composite sheets and leading to an excellent selectivity for a particular gas molecule. These preliminary sensing performance results indicate that the as-prepared composite can potentially be used as a highly efficient CTL sensing material for detecting propanal.

For comparison, we also investigated the responses of the as-prepared SnO_2/graphene composite and pure SnO_2 to propanal with same concentration under the same CTL test conditions. Pure SnO_2 was obtained *via* heating the composite at 500 °C in an oxygen atmosphere for 6 h to remove graphene, as shown in Fig. S3,† the structure, size and morphology of SnO_2 nanocrystals basically doesn't change after removal of graphene, however, serious aggregation problem appears which greatly reduced the surface area of sensing material and was one of the reasons for lowering the catalytic activity for propanal oxidation. As presented in Fig. 4c, the SnO_2/graphene composite exhibits a much higher intensity, and much faster response and recovery than pure SnO_2 nanoparticles, although the amount of SnO_2 in the composite was less than that of pure SnO_2 nanoparticles.

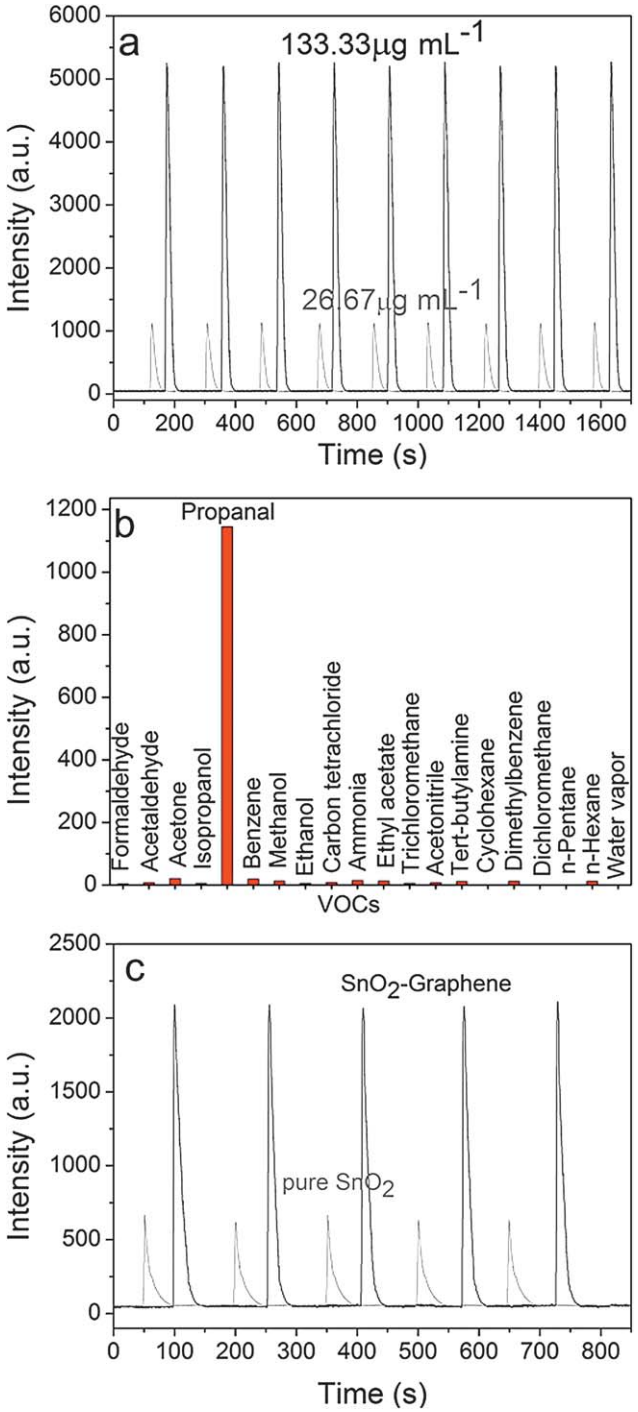

Fig. 4 (a) Response curves of the CTL sensor based on SnO_2/graphene composite to propanal at two different concentrations: 26.67 μg mL^{-1} and 133.33 μg mL^{-1}. Flow rate of carrier gas: 300 mL min^{-1}; temperature of the CTL sensor: 493 K. (b) The selectivity towards propanal of the prepared CTL sensor based on SnO_2/graphene composite. The concentration of propanal: 26.67 μg mL^{-1}; the concentration of others: about 200 μg mL^{-1}; flow rate of carrier gas: 300 mL min^{-1}; temperature of the CTL sensor: 573 K. (c) Response curves of the CTL sensor based on SnO_2/graphene and pure SnO_2 nanoparticles to propanal with a concentration of 53.33 μg mL^{-1}; Flow rate of carrier gas: 300 mL min^{-1}; The temperature of CTL sensor: 533 K.

It means that the introduction of graphene into the composite plays an important role in the superior CTL sensing performance for propanal. As described above, small SnO_2 nanoparticles are exclusively deposited on graphene sheets with high density and high uniformity, resulting in more porosity and large specific surface area which can provide additional adsorption sites for accommodation of O_2 and facilitate the rapid oxidation of propanal when it passed through the sensing system. Moreover, SnO_2 connecting to graphene sheets may have a synergetic effect, which can also improve the reaction rate of propanal oxidation. Therefore, the prepared composite results in the enhancement of cataluminescence properties and will be a novel highly efficient CTL sensing material due to the graphene sheets with outstanding physicochemical properties.

The analytical characteristics of the CTL sensor based on SnO_2/graphene composite have been examined under the optimal conditions (Fig. S4 and Fig. S5, ESI†). Fig. 5 shows the typical CTL spectra and the reproducibility of responses of the as-designed CTL senor for propanal with a series of different concentrations, the calibration curve with a linear dynamic range of 1.34–266.67 μg mL^{-1} for propanal was also obtained (inset). The linear regression equation is $I = 38.47C + 96.45$ ($r = 0.9987$), where I is the average CTL intensity of replicate tests at same concentration level and C is the concentration of propanal vapor. The relative standard deviations (R.S.D.) of the CTL intensity at each concentration level shown in Fig. 4a and Fig. 5 are all less than 4%, which represents the good repeatability of this determination method. Compared to other methods of determination of propanal,[44,45] the present method with a detection limit of 0.3 μg mL^{-1} ($S/N = 3$) and linear ranges magnitude of two orders shows superior analytical performances. The stability and durability of the CTL sensor based on SnO_2/graphene composite were also examined. The CTL intensity was detected for a week by continuously introducing 26.67 μg mL^{-1} propanal in the air carrier through the sensor. No significant decrease of CTL intensity was observed during a week and the R.S.D. is less than

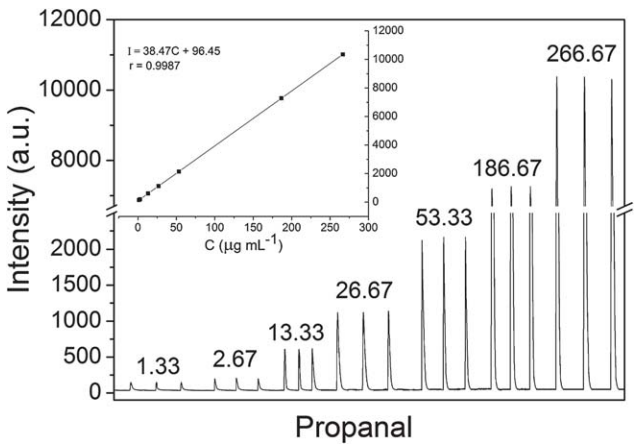

Fig. 5 Typical CTL spectra and the reproducibility of responses of the present CTL senor for propanal with a series of different concentrations, the inset is the calibration curve and the linear regression equation. I: the average CTL intensity of replicate tests at same concentration level; C: the concentration of propanal vapor. Flow rate of carrier gas: 300 mL min^{-1}; The temperature of CTL sensor: 513 K.

5%, suggestive of good stability and relatively long-time durability.

4. Conclusions

Successful preparation of SnO_2/graphene composite is very meaningful both for fundamental study of graphene-based composites and for practical application. We reported a facile strategy to synthesize graphene sheets decorated with SnO_2 nanocrystals through a hydrothermal-assisted oxidation-reduction reaction route. The key to this method is the *in situ* formation of SnO_2 nanocrystals and graphene sheets simultaneously, which can decrease the serious stacking of graphene sheets and prevent the agglomeration of SnO_2 nanoparticles. Moreover, we developed a new application domain for graphene-based composite, SnO_2/graphene composite was found to be a highly efficient material for CTL sensor to propanal. Because of its excellent analytical performance, the fabricated CTL sensor device is potentially applicable for the *in situ* detection of propanal in monitoring on environment.

Acknowledgements

This work was supported by the National Nature Science Foundation of China (20835003 & 21075084) and the Sichuan Youth Science & Technology Foundation (No. 2009-18-409). The authors also gratefully thank Dr Jiqiu Wen, Dr Shanling Wang, and Dr Hong Chen of Analytical & Testing Center at Sichuan University for assistance with the XRD, HRTEM and XPS analysis.

References

1 K. S. Novoselov, A. K. Geim, S. V. Morozov, D. Jiang, M. I. Katsnelson, I. V. Grigorieva, S. V. Dubonos and A. A. Firsov, *Nature*, 2005, **438**, 197–200.
2 Y. B. Zhang, Y. W. Tan, H. L. Stormer and P. Kim, *Nature*, 2005, **438**, 201–204.
3 A. K. Geim and K. S. Novoselov, *Nat. Mater.*, 2007, **6**, 183–191.
4 A. H. Castro Neto, F. Guinea, N. M. R. Peres, K. S. Novoselov and A. K. Geim, *Rev. Mod. Phys.*, 2009, **81**, 109–162.
5 C. Berger, Z. M. Song, T. B. Li, X. B. Li, A. Y. Ogbazghi, R. Feng, Z. T. Dai, A. N. Marchenkov, E. H. Conrad, P. N. First and W. A. de Heer, *J. Phys. Chem. B*, 2004, **108**, 19912–19916.
6 X. R. Wang, Y. J. Ouyang, X. L. Li, H. L. Wang, J. Guo and H. J. Dai, *Phys. Rev. Lett.*, 2008, **100**, 206803.
7 S. Gilje, S. Han, M. Wang, K. L. Wang and R. B. Kaner, *Nano Lett.*, 2007, **7**, 3394–3398.
8 H. K. Chae, D. Y. Siberio-Perez, J. Kim, Y. Go, M. Eddaoudi, A. J. Matzger, M. O'Keeffe and O. M. Yaghi, *Nature*, 2004, **427**, 523–527.
9 Y. C. Si and E. T. Samulski, *Chem. Mater.*, 2008, **20**, 6792–6797.
10 G. Williams, B. Seger and P. V. Kamat, *ACS Nano*, 2008, **2**, 1487–1491.
11 J. B. Liu, S. H. Fu, B. Yuan, Y. L. Li and Z. X. Deng, *J. Am. Chem. Soc.*, 2010, **132**, 7279–7281.
12 C. Xu, X. Wang and J. W. Zhu, *J. Phys. Chem. C*, 2008, **112**, 19841–19845.
13 G. Goncalves, P. Marques, C. M. Granadeiro, H. I. S. Nogueira, M. K. Singh and J. Gracio, *Chem. Mater.*, 2009, **21**, 4796–4802.
14 R. Pasricha, S. Gupta and A. K. Srivastava, *Small*, 2009, **5**, 2253–2259.
15 X. Z. Zhou, X. Huang, X. Y. Qi, S. X. Wu, C. Xue, F. Y. C. Boey, Q. Y. Yan, P. Chen and H. Zhang, *J. Phys. Chem. C*, 2009, **113**, 10842–10846.
16 Y. K. Kim, H. K. Na, Y. W. Lee, H. Jang, S. W. Han and D. H. Min, *Chem. Commun.*, 2010, **46**, 3185–3187.
17 J. Li and C. Y. Liu, *Eur. J. Inorg. Chem.*, 2010, 1244–1248.
18 F. Liu, J. Y. Choi and T. S. Seo, *Chem. Commun.*, 2010, **46**, 2844–2846.
19 Z. G. Xiong, L. L. Zhang, J. Z. Ma and X. S. Zhao, *Chem. Commun.*, 2010, **46**, 6099–6101.
20 Y. G. Zhou, J. J. Chen, F. B. Wang, Z. H. Sheng and X. H. Xia, *Chem. Commun.*, 2010, **46**, 5951–5953.
21 F. H. Li, J. F. Song, H. F. Yang, S. Y. Gan, Q. X. Zhang, D. X. Han, A. Ivaska and L. Niu, *Nanotechnology*, 2009, **20**, 455602.
22 G. Williams and P. V. Kamat, *Langmuir*, 2009, **25**, 13869–13873.
23 H. P. Cong, J. J. He, Y. Lu and S. H. Yu, *Small*, 2010, **6**, 169–173.
24 Y. C. Fan, L. J. Wang, J. L. Li, J. Q. Li, S. K. Sun, F. Chen, L. D. Chen and W. Jiang, *Carbon*, 2010, **48**, 1743–1749.
25 L. S. Zhang, L. Y. Jiang, H. J. Yan, W. D. Wang, W. Wang, W. G. Song, Y. G. Guo and L. J. Wan, *J. Mater. Chem.*, 2010, **20**, 5462–5467.
26 X. Y. Zhang, H. P. Li, X. L. Cui and Y. H. Lin, *J. Mater. Chem.*, 2010, **20**, 2801–2806.
27 C. Z. Zhu, S. J. Guo, P. Wang, L. Xing, Y. X. Fang, Y. M. Zhai and S. J. Dong, *Chem. Commun.*, 2010, **46**, 7148–7150.
28 G. X. Zhu, Y. J. Liu, Z. Xu, T. A. Jiang, C. Zhang, X. Li and G. Qi, *ChemPhysChem*, 2010, **11**, 2432–2437.
29 J. W. Zhu, G. Y. Zeng, F. D. Nie, X. M. Xu, S. Chen, Q. F. Han and X. Wang, *Nanoscale*, 2010, **2**, 988–994.
30 Z. F. Du, X. M. Yin, M. Zhang, Q. Y. Hao, Y. G. Wang and T. H. Wang, *Mater. Lett.*, 2010, **64**, 2076–2079.
31 J. Yao, X. P. Shen, B. Wang, H. K. Liu and G. X. Wang, *Electrochem. Commun.*, 2009, **11**, 1849–1852.
32 S. M. Paek, E. Yoo and I. Honma, *Nano Lett.*, 2009, **9**, 72–75.
33 B. Li, G. Sauvé, M. C. Iovu, M. Jeffries-El, R. Zhang, J. Cooper, S. Santhanam, L. Schultz, J. C. Revelli, A. G. Kusne, T. Kowalewski, J. L. Snyder, L. E. Weiss, G. K. Fedder, R. D. McCullough and D. N. Lambeth, *Nano Lett.*, 2006, **6**, 1598–1602.
34 Z. Y. Zhang, C. Zhang and X. R. Zhang, *Analyst*, 2002, **127**, 792–796.
35 X. Wang, N. Na, S. C. Zhang, Y. Y. Wu and X. R. Zhang, *J. Am. Chem. Soc.*, 2007, **129**, 6062–6063.
36 Y. Y. Wu, N. Na, S. Zhang, X. Wang, D. Liu and X. R. Zhang, *Anal. Chem.*, 2009, **81**, 961–966.
37 L. C. Zhang, Q. Zhou, Z. H. Liu, X. D. Hou, Y. B. Li and Y. Lv, *Chem. Mater.*, 2009, **21**, 5066–5071.
38 M. R. Almasian, N. Na, F. Wen, S. C. Zhang and X. R. Zhang, *Anal. Chem.*, 2010, **82**, 3457–3459.
39 J. Hu, K. L. Xu, Y. Z. Jia, Y. Lv, Y. B. Li and X. D. Hou, *Anal. Chem.*, 2008, **80**, 7964–7969.
40 G. M. Scheuermann, L. Rumi, P. Steurer, W. Bannwarth and R. Mulhaupt, *J. Am. Chem. Soc.*, 2009, **131**, 8262–8270.
41 L. S. Zhong, J. S. Hu, Z. M. Cui, L. J. Wan and W. G. Song, *Chem. Mater.*, 2007, **19**, 4557–4562.
42 G. X. Wang, B. Wang, X. L. Wang, J. Park, S. X. Dou, H. Ahn and K. Kim, *J. Mater. Chem.*, 2009, **19**, 8378–8384.
43 Y. D. Wang, I. Djerdj, B. Smarsly and M. Antonietti, *Chem. Mater.*, 2009, **21**, 3202–3209.
44 T. Sahm, A. Gurlo, N. Barsan and U. Weimar, *Part. Sci. Technol.*, 2006, **24**, 441–452.
45 A. B. de Carvalho, M. Kato, M. M. Rezende, P. Pereira and J. B. de Andrade, *J. Sep. Sci.*, 2008, **31**, 1686–1693.